Calculation of the electronic properties of Mo in a first-principles nonlocal-pseudopotential approach

Alex Zunger,* G. P. Kerker,† and Marvin L. Cohen
Department of Physics, University of California, Berkeley, California 94720
and Materials and Molecular Research Division, Lawrence Berkeley Laboratory, Berkeley, California 94720
(Received 8 September 1978)

The first-principles nonlocal atomic pseudopotentials previously derived from the density-functional formalism are applied in a self-consistent study of the electronic properties of bulk Mo. Using a mixed-basis representation for the crystalline wave functions, both the localized and the extended features of the electronic states are efficiently described. We show that by use of a completely nonempirical approach the basic electronic properties of the system, such as the band structure, density of states, charge density, and Fermi surface, are favorably reproduced within the pseudopotential formalism.

I. INTRODUCTION

The pseudopotential method which has been successfully applied to the study of electronic and structural properties of many nontransition-metal systems,[1] has recently been extended to transition metals.[2–7] This case is more difficult in general because of the inadequacy of perturbative approaches[8] to the strong transition-metal core pseudopotentials, the inefficiency of a plane-wave basis set for describing the localized features of the d-wave functions, and the pronounced orbital nonlocality of the pseudopotentials. In addition, an empirical parametrization of the bare-ion potential[9] has been largely inhibited by the incompleteness of the measured single-valence electron term value spectra of transition metals. Despite the difficulties, non-self-consistent empirical pseudopotential calculations have been carried out on a number of transition metals[2–5] by fitting the observed optical reflectivity of the bulk solids. Although generally good agreement is obtained with the experimental spectra and Fermi surface, the underlying pseudopotentials are only partially successful when transferred to study the electronic properties of phases which are substantially different from the reference system used for fitting the potential (i.e., the bulk elemental solid). This results from the fact that in the empirical approach both the core pseudopotential and the (dynamic) valence screening fields (interelectronic Coulomb and exchange) are combined together to *a charge-density independent* form $V_{\text{emp}}(\vec{G})$ which in turn is adjusted to fit some bulk properties. As no attempt is made to feed back the variational crystal charge density into $V_{\text{emp}}(\vec{G})$, the latter cannot effectively describe the charge relaxation in systems different from the reference one.

Recently,[10–12] we have presented a new class of nonlocal atomic pseudopotentials for the first five rows of the Periodic Table, which are self-consistently derived from the density-functional representation[13] to the all-electron system. These pseudopotentials involve no (prefixed or adjustable) parameters other than the atomic number. In their derivation, no fitting to either atomic or solid-state experimental data is needed. Instead, they are obtained by a direct inversion of the density-functional effective single-particle equation pertaining to a pseudo atom characterized by local-density Coulomb and exchange-correlation interaction and the (yet unspecified) nonlocal static external field $V_l(r)$. The pseudopotential $V_l(r)$ is then solved for under the constraints that: (i) the ground-state valence energy eigenvalue spectra of the pseudo atom be identical to that of the all-electron atom characterized by the same form of density functionals and (ii) the wave-function pseudizing process is described by a unitary rotation in the subspace of occupied all-electron ("true") orbitals, $\psi_{nl}(r)$, i.e., the pseudo wave functions $\chi_{nl}(r)$ are given as a linear combination of both core and valence functions $\psi_{n'l}(r)$ with coefficients $C^{(l)}_{n,n'}$. These rotation coefficients are then fixed by requiring that the pseudo wave functions be (a) nodeless for each of the lowest solutions of every symmetry, (b) normalized, and (c) have the maximum similarity possible under conditions (a) and (b) to the "exact" all-electron density-functional wave functions $\psi_{nl}(r)$ in the valence region. When additional degrees of freedom are available (e.g., systems having more than one core orbital) an additional minimum radial kinetic energy constraint is imposed. The reader is referred to previous articles[10,11] for the detailed discussion of the choice of this physical model.

This approach not only assures that both the energies *and the wave functions* of the pseudo Hamiltonian closely resemble the corresponding all-electron results for the reference ground-state atom, but also results in a very *small energy dependence* of the pseudopotential: when a ground-state first-principles pseudopotential is applied to calculate electronic properties of excited species (having very different wave functions

and energies) good agreement ($\sim 10^{-3}$ Hartrees) with all-electron results is found over a large range of excitation energies. We have recently applied these pseudopotentials to study phase stabilities of binary solids[14] and to electronic properties of semiconductors.[15]

In contrast to the semiempirical pseudopotential approach,[6,7] the first-principles pseudopotential method does not assume any ansatz form for $V_l(r)$. In turn, its shape both in the core and the valence regions is automatically determined (numerically) by the maximum similarity and minimum kinetic energy constraints. We find that these potentials are strongly repulsive in the core regions, quantitatively reflecting the effects of the replacement of the radial nodes in the all-electron wave functions by nodeless, smooth maximum-similarity pseudo wave functions. We find in fact that this repulsiveness, as reflected in the occurrence of zero-energy turning points r_l of the screened pseudopotentials [where $V_l(r)=0$], scales with the generalized l-dependent electronegativity of the atom and provides a remarkably accurate phase separation of both octet and suboctet binary systems.[14] This small r repulsiveness in general produces crystal wave functions that do not lend themselves to a rapidly convergent Fourier representation.[16] In some simple applications to bulk Si,[15] and to diatomic molecules such as O_2,[17] and Si_2,[18] we find in fact that these high-momentum components of the wave functions are indeed needed for an adequate representation of the charge anisotropy in the bond region. Using a Gaussian–plane-wave mixed-basis representation[19–22] to the crystalline wave functions, both the localized and the extended features of the electronic states are accurately described.

The differences between the semiempirical and the first-principles pseudopotentials in the core region might at first seem irrelevant to the properties of the *valence* electrons. They are however related to the important energy dependence of the pseudopotentials. When used in self-consistent field calculations for systems other than those used for fixing the potential (e.g., ground-state atom) the "softness" of the model semiempirical potentials[6,7] in the core regions allows a flow of excess *valence* charge into the core region, where the underlying frozen core pseudopotential description is least valid. Hence, whereas the model potential well describes (by definition) the reference system used for its construction, it is implicitly energy dependent in that its description of perturbed systems (e.g., excited atoms, molecules, etc.) gets progressively poorer as the perturbing energy increases. In contrast, the repulsiveness of the first-principles potentials in the core regions allows only minor penetration of the valence states into the core region via low-probability tunneling, resulting thereby in a very small energy dependence. This point is further illustrated below.

In this paper we present the results for the band structure, density of states, Fermi surface, and charge density for bcc molybdenum using the first-principles pseudopotential. Using the mixed-basis representation, the angular-momentum nonlocality of the pseudopotentials is taken into account in a simple manner. As the calculation is carried out in reciprocal space, the conventional muffin-tin approximation to the charge density and potential is completely avoided. Extension to the calculation of the bulk ground-state properties (equilibrium lattice constant, cohesive energy, and bulk modulus) are presented in a separate publication.[23]

The electronic structure of Mo has been previously calculated by the augmented-plane-wave (APW) method by Loucks,[24] Petroff and Viswanathan,[25] and Cinti *et al.*[26] All these were carried out in a non-self-consistent manner using the spherically symmetric muffin-tin part of the superposition of free-atom charge densities. Koelling *et al.*[27] have performed a relativistic APW calculation and included non-muffin-tin corrections between the spheres. Iverson and Hodges[28] have performed a renormalized-atom calculation, while recently, Moruzzi *et al.*[29] have reported a self-consistent muffin-tin Korringa-Kohn-Rostoker (KKR) energy-band calculation. None of the above mentioned calculations have reported the charge-density results while only the calculation by Petroff and Viswanathan[25] and Cinti *et al.*[26] included some optical results. A more detailed study of the optical properties of Mo has been performed by Pickett and Allen[30] based on the APW results of Petroff and Viswanathan.

II. METHOD OF CALCULATION

A. The pseudopotential

We have used the first-principles Mo pseudopotential developed in Refs. 10-12. The method of generating such pseudopotentials has been previously described and will not be repeated here. Figure 1 shows the components of the nonlocal Mo potential.

The adequacy of these potentials can be partially assessed by comparing the exact *all-electron* atomic results with those obtained from a similarly self-consistent (numerical) *pseudopotential* calculation. Such a comparison is given in Table I, from which it is clear that not only the pseudopotential energy eigenvalues match very accurately those of the all-electron results, but that the orbital moments are similarly very close. As the pseudo wave functions are represented in this formalism as a unitary rotation in the space of the true all-electron wave functions,[10,11] core orthogonalization of the former reproduces the exact results (aside from numerical errors, cf. Table I). This feature is not enjoyed by any of

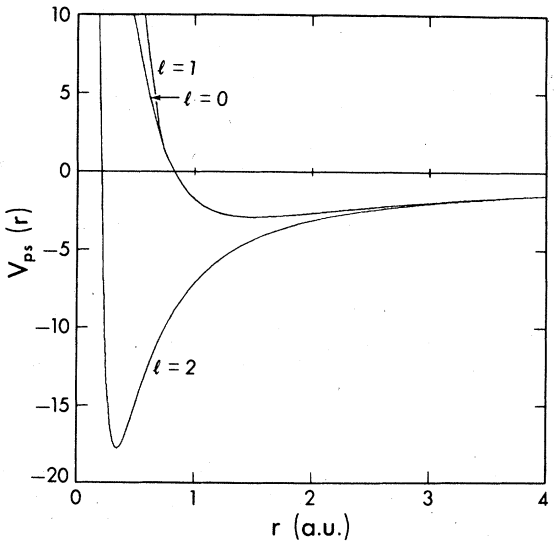

FIG. 1. First-principles nonlocal pseudopotential of Mo (Ref. 11).

the empirical or semiempirical pseudopotentials. Even more strikingly, we find that application of these Mo pseudopotentials (derived from the ground-state atomic wave functions) to excited configurations (e.g., Mo $5s^25p^14d^3$, Mo $5s^15p^14d^4$, Mo $5s^05p^04d^6$, Mo^{1+} $5s^25p^04d^2$, and Mo^{1+} $5s^15p^04d^4$) produces energy eigenvalues and orbital moments $\langle r\rangle$ that deviate by less than 1 and 5%, respectively, from the corresponding all-electron results. This confirms the low-energy (and state) dependence of these pseudopotentials and the underlying insensitivity of the core potentials to changes in the valence configuration. We find that whereas the fitting of the pseudopotential to simple analytic forms (designed primarily to produce a fast convergence in momentum space, e.g., Refs. 6, 7) might introduce an unwarranted energy dependence,[31] its form-unrestricted generation directly from the variational eigenvalue problem[10–12] yields a nearly energy independent and accurate potential.

The pseudopotentials shown in Fig. 1 are much deeper and more localized than those pertaining to nontransition elements.[1] The depth of the $l=0$, 1, and 2 potentials is −5.80, −5.77, and −35.54 Ry, respectively, and the classical turning points occur at 0.84, 0.89, and 0.20 a.u., respectively. Clearly, the conventional plane-wave representation of the crystalline wave functions is largely ineffective for such systems. We next discuss the mixed-basis representation[19] for the electronic states.

B. Eigenvalue problem

The crystalline wave function $\chi_j(\vec{k},\vec{r})$ for the Brillouin zone (BZ) wave vector $\vec{k}$ and band j is represented here as a sum of a plane-wave part and localized LCAO (linear combination of atomic orbitals) Bloch functions $\Phi_{\mu\alpha}(\vec{k},r)$,[19–22]

$$\chi_j(\vec{k},\vec{r}) = \sum_{\vec{G}} C^{(j)}_{\vec{k}+\vec{G}} e^{i(\vec{k}+\vec{G})\cdot\vec{r}} + \sum_{\mu}\sum_{\alpha} D^{(j)}_{\mu\alpha}(\vec{k})\Phi_{\mu\alpha}(\vec{k},\vec{r}) \ , \quad (1)$$

where $C^{(j)}_{\vec{k}+\vec{G}}$ and $D^{(j)}_{\mu\alpha}(\vec{k})$ are the expansion coefficients determined variationally. The LCAO Bloch function $\Phi_{\mu\alpha}(\vec{k},\vec{r})$ is constructed from the μth basis function on sublattice α as

$$\Phi_{\mu\alpha}(\vec{k},\vec{r}) = N^{-1/2}\sum_{n} e^{i\vec{k}\cdot\vec{R}_n} d_{\mu\alpha}(\vec{r}-\vec{R}_n-\vec{\tau}_\alpha) \ , \quad (2)$$

TABLE I. Comparison between the energy eigenvalues (in eV) and orbital moments $\langle r\rangle$ and $\langle r^2\rangle$ (in a.u. and a.u.^{2}, respectively) of the exact all-electron, the pseudopotential, and the core orthogonalized pseudopotential for the $5s^25p^04d^4$ state of Mo.

Property	All-Electron	pseudopotential	Core orthogonalized Pseudopotential
$\epsilon 5s$	−3.9329	−3.9330	
$\epsilon 5p$	−0.8838	−0.8838	
$\epsilon 4d$	−5.1143	−5.1142	
$\langle r\rangle_{5s}$	3.5666	3.4163	3.5664
$\langle r\rangle_{5p}$	5.2169	5.1089	5.2168
$\langle r\rangle_{4d}$	1.8557	1.7997	1.8556
$\langle r^2\rangle_{5s}$	14.6555	13.9677	14.6551
$\langle r^2\rangle_{5p}$	32.5897	32.0041	32.5898
$\langle r^2\rangle_{4d}$	4.2706	4.1341	4.2703

where $\vec{R}_n$ and $\vec{\tau}_\alpha$ denote the direct primitive lattice vector and the sublattice coordinate, respectively, and N is a normalization constant. The basis orbitals $d_{\mu\alpha}(\vec{r})$ are chosen as a linear combination of Gaussians as

$$d_{\mu\alpha}(\vec{r}) = N_{lm} r^l K_{lm}(\theta,\phi) \sum_i a_{lm\alpha}^{(i)} e^{-\gamma_i r_i^2} \quad , \tag{3}$$

where N_{lm} is a normalization, $K_{lm}(\theta,\phi)$ are the Kubic harmonics of angles θ and ϕ, and μ denotes the indices l and m collectively. The contracted coefficients $a_{lm\alpha}^{(i)}$ are determined from the outset such that $d_{\mu\alpha}(r)$ have desired properties (e.g., fit the small r behavior of the atomic pseudo wave functions).

In the present approach we expand the LCAO Bloch functions in a Fourier series as

$$\Phi_{\mu\alpha}(\vec{k},\vec{r}) = M^{-1/2} \sum_{\vec{G}} e^{i(\vec{k}+\vec{G})\cdot\vec{\tau}} d_{\mu\alpha}(\vec{k}+\vec{G}) T_\alpha(\vec{G}) \quad , \tag{4}$$

where M is a normalization constant, $d_{\mu\alpha}(\vec{k}+\vec{G})$ is the Fourier transform of the basis orbital $d_{\mu\alpha}(r)$ (obtained readily in closed form for either Gaussians or Slater-type basis orbitals), and $T_\alpha(\vec{G})$ is the structure factor

$$T_\alpha(\vec{G}) = \sum_p e^{-i\vec{G}\cdot\vec{\tau}_{\alpha,p}} \quad , \tag{5}$$

obtained by summing over all atoms p belonging to the αth sublattice.

The screened effective potential is given in the density-functional approach as

$$W(\vec{r}) = V_{ps}(\vec{r}) + V_{Coul}(\vec{r}) + V_x(\vec{r}) + V_{corr}(\vec{r}) \quad . \tag{6}$$

The core pseudopotential $V_{ps}(\vec{r})$ can be separated for convenience into a local part $V_L(\vec{r})$ and a nonlocal part $V_{NL}(\vec{r})$

$$V_{ps}(\vec{r}) = \sum_p \sum_l V_l(\vec{r}-\vec{R}_p)\hat{P}_l \equiv V_L + V_{NL}$$

$$= V_L + \sum_p \sum_l [V_l(\vec{r}-\vec{R}_p) - V_L]\hat{P}_l \quad , \tag{7}$$

such that V_L is smooth in momentum space, while V_{NL} is localized in direct space. Here $V_l(\vec{r})$ denotes the atomic pseudopotentials (Fig. 1) and $\hat{P}_l$ is the core projection operator. The interelectronic Coulomb screening is related to the variational charge density

$$\rho(\vec{r}) = \sum_{j,k} N_j(\vec{k}) |\chi_j^*(\vec{k},\vec{r})\chi_j(\vec{k},\vec{r})| \tag{8}$$

by the Poisson equation

$$V_{Coul}(\vec{r}) = \int \frac{\rho(\vec{r}')}{|\vec{r}-\vec{r}'|} d\vec{r}' \quad , \tag{9}$$

whereas the exchange (V_x) and correlation (V_{corr}) potentials are nonlinear functionals of the density $\rho(\vec{r})$ for which we choose the Kohn and Sham[11] $\rho^{1/3}(r)$ form (with an exchange coefficient of $\alpha = \frac{2}{3}$) and the Singwi *et al.*[32] form, respectively.

Within the plane-wave form of the total wave function [Eqs. (1) and (4)], the matrix representation of the potential (6) is very easily evaluated.[19] The element between two localized Bloch functions is

$$\langle \Phi_{\mu\alpha}(\vec{k},\vec{r}) | W(\vec{r}) | \Phi_{\nu\beta}(\vec{k},\vec{r}) \rangle = \sum_{\vec{G}} \sum_{\vec{G}'} T_\alpha(\vec{G}) T_\beta(\vec{G}') d_{\mu\alpha}(\vec{k}+\vec{G}) d_{\nu\beta}(\vec{k}+\vec{G}') \langle \vec{k}+\vec{G} | W(r) | \vec{k}+\vec{G}' \rangle \quad , \tag{10}$$

where,

$$\langle \vec{k}+\vec{G} | W(\vec{r}) | \vec{k}+\vec{G}' \rangle = \langle \vec{k}+\vec{G} | V_L + V_{Coul} + V_x + V_{corr} | \vec{k}+\vec{G}' \rangle \delta_{\vec{G}\vec{G}'} + \langle \vec{k}+\vec{G} | V_{NL} | \vec{k}+\vec{G}' \rangle \quad . \tag{11}$$

The first matrix element is obtained by first representing the screening field $V_L + V_{Coul} + V_x + V_{corr}$ in a Fourier series [by fast Fourier transforming[33] $V_x(\vec{r})$, $V_{corr}(\vec{r})$, and $\rho(\vec{r})$ and obtaining $V_{Coul}(\vec{Q})$ as $\rho(\vec{Q})/|\vec{Q}^2|$] while the off-diagonal second element is obtained by analyzing the plane waves $|\vec{k}+\vec{G}\rangle$ in a partial wave and Bessel series

$$\langle \vec{k}+\vec{G} | V_{NL} | \vec{k}+\vec{G}' \rangle = \frac{4\pi}{\Omega} \sum_\alpha S_\alpha(\vec{G}-\vec{G}') \sum_l (2l+1) P_l(\cos\theta \vec{G}\cdot\vec{G}') F_l(k+G, k+G') \quad , \tag{12}$$

where S_α is the structure factor and P_l is the Legendre polynomial. The quantity $F_l(Q,Q')$ is obtained by a simple radial integration

$$F_l(Q,Q') = \langle j_l(|Qr|) | V_{NL} | j_l(|Q'r|) \rangle \quad . \tag{13}$$

In the present calculation we choose as the local potential V_L the $l=0$ component of the pseudopotential.[34] We use $l=2$ as the highest angular momentum component of the pseudopotential, as higher momenta probably contribute very little to the crystalline wave function at the energy range of interest. The nonlocal potential V_{NL} hence has an s-p and an

s-d contribution. Figure 2 shows a contour plot of the corresponding momentum representation of $F_l(Q,Q')$ for $l=1$ and 2. It is seen that these contributions peak at about $Q=Q'=7.35$ a.u.$^{-1}$ for the s-p nonlocality (with a secondary minimum at $Q=Q'=0.5$ a.u.$^{-1}$) while the s-d nonlocality has a single maximum at $Q=Q'=2.76$ a.u.$^{-1}$ and decays monotonically at higher momenta. Most of the strong scattering events occur along the $Q=Q'$ line for the s-d nonlocality while the s-p nonlocality is seen to scatter effectively for almost all $\vec{Q}-\vec{Q}'$ directions. Only the low momentum extrema of the s-p nonlocality is important in determining the band structure as the secondary maxima occurs in a momentum region where the (repulsive) kinetic contributions (or order $|\vec{Q}-\vec{Q}'|^2$) are dominant. The local pseudopotential $V_L(Q)=V_{l=0}(Q)$ and the off-diagonal nonlocal matrices $F_1(Q,Q')$ and $F_2(Q,Q')$ form the only input (other than the lattice structure) to this calculation. These are in turn simply determined by the first-principles atomic pseudopotentials.[10,11]

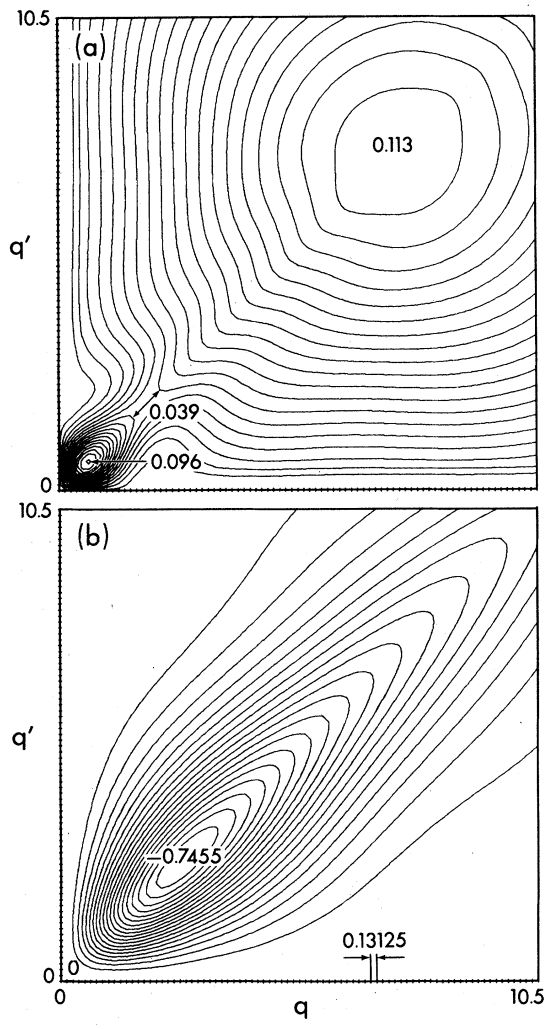

FIG. 2. Contour plots of the momentum representation of the nonlocal Mo pseudopotential [Eq. (13)]. (a) $F_1(q,q')$ contour step $=0.0057$ Ry. (b) $F_2(q,q')$ contour step $=0.0373$ Ry.

The other relevant matrix elements (overlap and kinetic energy) are trivial and will not be discussed here.

The variational charge density [Eq. (8)] is obtained by evaluating the symmetrized wave functions $\chi_j(\vec{k},\vec{r})$ over a grid in the irreducible BZ. Whereas in insulators and semiconductors it is possible to use the "special $\vec{k}_p$ points"[35] with their associated weights $W(\vec{k}_p)$, the presence of a Fermi surface in metals requires a generalization of these to both wave vector and *band* dependent weights $W_j(\vec{k}_p)$.[36] We hence sample the irreducible BZ into 32 tetrahedra and used the energy eigenvalues at the tetrahedra corners to evaluate the density of states and Fermi energy ϵ_F, at a given interation.[37] The weights $W_j(\vec{k}_p)$ are then evaluated from the fraction of each tetrahedron which lies below ϵ_F. These are then used to replace the Fermi-Dirac occupation numbers $N_j(\vec{k})$ in Eq. (8). Table II gives the final weights obtained from the self-consistent results at 14 $\vec{k}_p$ points in the irreducible zone. It is clear from this table that the weights associated with the upper three bands vary considerably with the band index for fixed $\vec{k}_p$ due to the complex features of the Fermi surface.

Adequate accuracy in the resulting band structure and charge density requires the establishment of a satisfactory convergence of the wave function and potential expansion. A judicious choice of the Gaussian exponents γ_i and contraction coefficients $a_{lm\alpha}^{(i)}$ in Eq. (3) would lead to a rather small number of plane waves in the basis (1), as more of the localized features of the wave function are represented by the real-space Bloch sums. While large Gaussian exponents would require high cutoff values in the Fourier expansion of $\Phi_{\mu\alpha}(\vec{k},\vec{r})$ [Eq. (4)], unduly small exponents might lead to approximate linear dependence in the basis (monitored by the smallness of the overlap matrix eigenvalues[38]). We find that the use of a single $l=2$-type Gaussian [i.e., $i=1$, and $-2\leq m\leq 2$ in Eq. (3)] with an exponent of 1.9 a.u.$^{-2}$ produces adequate convergence of the wave function over the entire BZ. With this choice, an accuracy of 0.05 eV in the energy eigenvalues requires approximately 90–100 plane waves in the basis [Eq. (1)] and 530 plane waves in the expansion of the localized Block functions [Eq. (4)]. As the size of the secular equation is determined by the former number, the relatively large cutoff associated with the expansion (4) poses no problem. For comparison, a similar accuracy in a pure plane-wave calculation [i.e., $D_{\mu\alpha}^{(j)}(\vec{k})\equiv 0$ in Eq. (1)] requires about 430 waves in

TABLE II. Self-consistent wave vector and band-dependent weights for Mo. The density is given as $\sum_j \sum_{\vec{k}_p} W_j(\vec{k}_p)|\chi_j^*(\vec{k}_p,\vec{r})\chi_j(\vec{k}_p,\vec{r})|$, where $\chi_j(\vec{k}_p,\vec{r})$ is the symmetrized wave function and the sum of weights is normalized to unity.

$\vec{k}_p$ point	band 1	band 2	band 3	band 4
$(\frac{1}{8},\frac{1}{8},-\frac{1}{8})$	0.020 833 3	0.020 833 30	0.020 833 00	0.005 692 60
$(0,\frac{1}{4},0)$	0.020 833 3	0.020 833 30	0.019 904 60	0.003 138 20
$(\frac{1}{8},\frac{1}{8},\frac{1}{8})$	0.031 250 0	0.031 250 00	0.031 250 00	0.003 555 30
$(\frac{1}{4},\frac{1}{4},-\frac{1}{4})$	0.020 833 3	0.020 833 30	0.020 032 40	0.003 159 20
$(\frac{1}{8},\frac{3}{8},-\frac{1}{8})$	0.041 666 0	0.041 666 00	0.039 931 80	0.003 565 40
$(\frac{1}{4},\frac{1}{4},0)$	0.052 083 3	0.052 083 30	0.050 367 50	0.003 334 40
$(0,\frac{1}{2},0)$	0.015 625 0	0.015 625 00	0.012 880 40	0.0
$(\frac{1}{8},\frac{3}{8},\frac{1}{8})$	0.036 458 3	0.036 458 30	0.034 519 86	0.0
$(\frac{1}{4},\frac{1}{4},\frac{1}{4})$	0.010 416 66	0.010 416 66	0.010 416 66	0.0
$(\frac{3}{8},\frac{3}{8},-\frac{3}{8})$	0.010 416 66	0.010 416 66	0.006 446 70	0.000 242 20
$(\frac{1}{4},\frac{1}{4},-\frac{1}{4})$	0.036 458 00	0.036 458 00	0.030 672 55	0.001 021 80
$(\frac{3}{8},\frac{3}{8},-\frac{1}{8})$	0.026 041 60	0.026 041 60	0.022 071 70	0.000 514 40
$(\frac{1}{2},\frac{1}{2},-\frac{1}{2})$	0.005 208 33	0.005 208 33	0.002 039 30	0.0
$(0,0,0)$	0.005 208 33	0.005 208 33	0.005 208 33	0.002 634 66

the wave-function expansion.

A compatible convergence in the Fourier representation of the potential and density requires larger cutoff values due to the contribution of back-scattering events. We find that about 959 plane waves are sufficient to produce the desired accuracy.

The calculation is initiated by approximating the effective potential $W(\vec{r})$ in Eq. (6) by a superposition of screened atomic pseudopotentials.[11] The energy eigenvalues and wave functions are then evaluated on a grid of points in the BZ (8 points for the initial iterations and 14 points for the last two), from which the density $\rho(\vec{r})$ [Eq. (8)] is evaluated. This is then used to calculate repeatedly the components of the screening field (6) until a consistency of about 10^{-3} Ry is obtained between successive iterations. The overall accuracy of the band structure is estimated to be about 0.1 eV.

III. RESULTS

A. Band structure

The self-consistent band structure of Mo obtained in the present exchange ($\alpha=\frac{2}{3}$) and correlation[32] density functional approach is given in Fig. 3. In

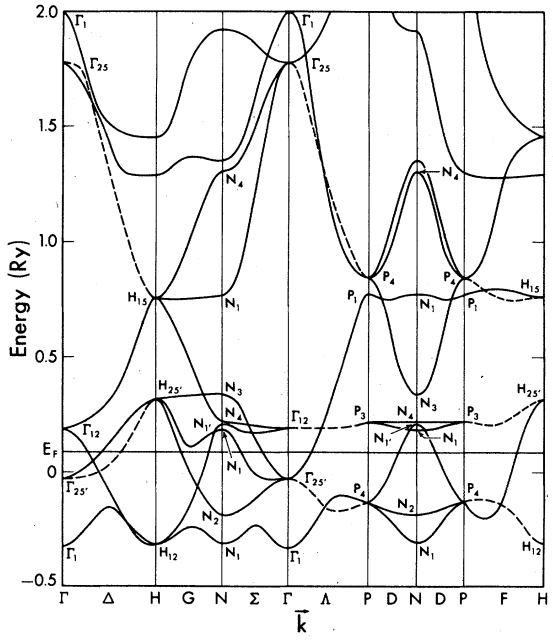

FIG. 3. Self-consistent nonlocal pseudopotential band structure of Mo in the exchange and correlation density-functional model. Dashed lines represent doubly degenerate representations.

Table III we have collected the energy eigenvalues at some high-symmetry points, relative to the calculated Fermi energy. The same table contains the results of three other studies for which energy-band eigenvalues have been previously published.[25,28,29,39]

Although the present results are qualitatively similar to most of the previously published results, few notable differences occur:

(i) The bottom of the s band at Γ_1 is substantially closer to the Fermi energy (and to the bottom of the d-based band at H_{12}) than in all other muffin-tin calculations, indicating larger s-d hybridization in the present results. The photoemission data of Kress and Lapeyre[40] seem to indicate an overall band with $\Gamma_1 - \epsilon_F$ somewhat below 6 eV, in better agreement with the present results. The bottom of the s band seems to be characteristic of the position of the element in the row of the Periodic Table as the $\Gamma_1 - \epsilon_F$ gap measures the relative binding energy of the $l=0$ state in these materials. This in turn reflects the variation in the strength of the $l=0$ pseudopotential: as one progresses down the row in the Periodic Table, the number of core states of $l=0$ symmetry increases and the pseudopotential cancellation for this symmetry improves, resulting in a weaker $l=0$ pseudopotential and a smaller s binding energy.[11] This observation is consistent with the reduced s binding energy found by us for W,[36] using a similar approach.

(ii) The p-like $N_{1'}$ state is lower than the corresponding state in other calculations and is split off from the d-like N_1 state more than in the APW results. This again implies more advanced p-d hybridization in the present calculation. Similarly, the excited N_1 state (seventh band) is substantially lower (2.4 eV) than the corresponding band in APW calculations. Cinti *et al.*[26] have observed that in order to get good agreement between their APW results and the photoemission data in the (110) polarization, the calculated value of this N_1 state has to be shifted downwards by about 3 eV, in agreement with the present results. An empirical pseudopotential calculation by Alward *et al.*[5] on row-V transition elements similarly suggests that the fitting of the observed reflectivity data for these materials in the energy range below 4 eV requires an adjustment of about 1.1 eV in the corresponding APW results for the $N_1 - N_{1'}$ gap (band $1-3$).

(iii) The relative separation of the P_4 ($d_{xy+yz+zx}$ symmetry) and the H_{12} state ($d_{z^2} + d_{x^2-y^2}$ symmetry) is smaller by about 1 eV in the present calculation relative to other results. Alward *et al.*[5] have noted that a reduction of 1–2 eV in this gap relative to APW results is in fact necessary in order to get an electrostatically stable ground-state charge distribution in row-V transition metals.

B. Density of states and the photoemission spectra

To obtain a density of states, the lowest ten energy bands were calculated for 35 independent $\vec{k}$ points in

TABLE III. Comparison between the present self-consistent exchange and correlation band eigenvalues of Mo and published results. All results are given in eV relative to the Fermi energy calculated by the respective authors.

State	APW Ref. 25	Renormalized Atom Refs. 28 and 39	KKR Ref. 29	Present Results
Γ_1	−6.64	−5.92	−6.50	−5.67
$\Gamma_{25'}$	−1.09	−1.49	−1.41	−1.52
Γ_{12}	1.46	1.37	1.34	1.51
Γ_{25}	14.93	· · ·	· · ·	23.25
H_{12}	−5.49	−6.24	−5.93	−5.21
$H_{25'}$	3.87	4.16	· · ·	3.21
H_{15}	9.51	· · ·	· · ·	9.21
N_1	−5.06	−5.52	−5.40	−5.42
N_2	−3.11	−3.71	−3.54	−3.61
$N_{1'}$	1.66	2.42	1.58	1.36
N_1	1.67	1.69	· · ·	1.68
N_4	2.18	2.27	· · ·	1.92
N_3	4.58	5.06	· · ·	3.63
N_1	11.85	· · ·	· · ·	9.41
P_4	−2.44	−2.62	−2.60	−2.88
P_3	2.29	2.35	· · ·	2.12
P_1	10.81	· · ·	· · ·	9.50

$\frac{1}{48}$ of the BZ and then transferred on a grid of 512 points throughout the whole zone by making use of the point group symmetries of the crystal. The Fourier coefficients of the energy bands

$$C_{\vec{R}}^{(n)} = \frac{1}{N} \sum_{\vec{K}} \epsilon_n(\vec{k}) e^{-\vec{k}\cdot\vec{R}} \quad , \tag{14}$$

were obtained using a fast Fourier transformation.[33] N is the number of grid points. The number of grid points R was then increased by a factor of 64 to a mesh of 32 768 points. Interpolated values for $\epsilon_n(\vec{k})$ are found by an inverse Fourier transformation on the large mesh setting $C_{\vec{R}}^{(n)} = 0$ on the additional points. The rms error of this interpolation scheme is less than 0.1 eV for all bands except at crossing points where the error can be of the order of 0.2 eV. In Table IV we compare for a k point which does not belong to the original 35 points the results of the fit with the energy bands calculated directly by solving the eigenvalue problem. The agreement is within less than 0.1 eV. The density of states is given by

$$D(\epsilon) = \frac{1}{N} \sum_{\vec{k},n} \delta(\epsilon - \epsilon_n(\vec{k})) \quad . \tag{15}$$

For the histogram in Fig. 4, we used an energy channel width of 0.1 eV. The Fermi energy ϵ_F is found from the integrated density of states

$$N(\epsilon) = \int^{\epsilon} D(\epsilon')\, d\epsilon' \quad , \tag{16}$$

using the criterion $N(\epsilon_F) = Z_v$, where Z_v is the number of (valence) electrons per atom ($Z_v = 6$ in the case of molybdenum).

The calculated density of states is shown in Fig. 4. Three main structures are observed below the Fermi energy and two peaks with 2 eV above E_F. These are compared in Table V with the available photoemission data.[40,41] The peaks at −3.96, −2.92, and −1.67 eV are very close to the high-symmetry points N_2 (d_{xy-zx}-type), P_4 ($d_{yz+zx+xy}$-type), and $\Gamma_{25'}$ ($d_{yz+zx+xy}$-type) while the doublet observed above

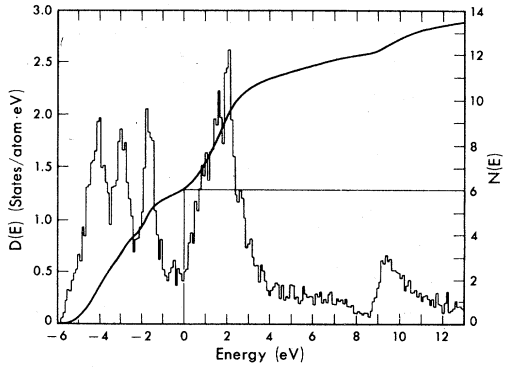

FIG. 4. Density of states of Mo and the electron number.

the Fermi energy coincides with the p-type $N_{1'}$ state and the d_{z^2}-type Γ_{12} state, respectively. The peaks below the Fermi energy are similarly close to the constant initial energy transitions (−3.5 and −1.7 eV) observed in the (100) polarized emission experiments of Cinti *et al.*[26] (peaks C and D). By varying the initial photon energy, Cinti *et al.*[26] were able to tentatively identify the location of the H_{12} (peak E, at −5 eV) and the $\Gamma_{25'}$ (peak B at −1.5 eV) states, in good agreement with the present results (−5.2 and −1.5 eV, respectively). An additional structure (A) at 0.5 eV below the Fermi energy[26,40] has been identified as a surface resonance state.

The reflectivity spectra of Mo has been previously obtained by a few workers. These include the study of Kirilova *et al.*[42] in the energy range below 4.9 eV, Kapitsa *et al.*[43] ($1.4 \leq \epsilon \leq 11$ eV), Veal and Paulikas[44] ($0.5 \leq \epsilon \leq 6$ eV) and Weaver *et al.*[45] ($0.1 < \epsilon < 35$ eV). No detailed analysis of these results is intended here. Instead, we will only comment on the assignment suggested by Weaver *et al.*[45] based on the muffin-tin non-self-consistent band structures available at that time.

Based on systematic comparisons with the spectra

TABLE IV. Comparison of Fourier fit with exact results for the energy bands of $\vec{K} = (0.1875, 0.031\,25, 0.3125)$.

Band	Eigenvalue [eV] exact	fit
1	−2.995 25	−2.929 44
2	−1.995 90	−1.991 16
3	0.056 410	0.004 08
4	2.809 92	2.834 7
5	3.458 12	3.449 87
6	6.872 74	6.920 89

TABLE V. Calculated and observed structures in the density of states of Mo, relative to the Fermi energy (in eV).

Photoemission Ref. 40	Photoemission Ref. 41	Present Results	APW Ref. 25
−3.9	−3.6	−3.96	−4.28
···	···	−2.92	−2.92
−1.6	−1.6	−1.63	−1.56
1.0	···	1.61	1.50
2.0	···	2.10	2.45

of V, Nb, and Ta, it has been suggested that the two prominent low-energy peaks at 2.35 and 4.1 eV arise from $\Sigma_1 \rightarrow \Sigma_1$ and $G_1 \rightarrow G_1$ transitions, respectively, while the wide absorption in the 11.5–20-eV region arises from transitions to unspecified empty d states. Using a minimum slope difference criteria between initial and final states, we find that the peak along $\Sigma_1 \rightarrow \Sigma_1$ should occur at 2.55 eV at about $\frac{1}{3}$ the distance from Γ to N and that a similar $G_1 \rightarrow G_1$ peak (bands 1 to 4) should occur at 4.55 eV at about half the distance between N and H. As the location of the high-energy unoccupied d states in this work is much higher than the corresponding quantity derived from APW results (compare Γ_{25} in Table III), the present result would predict strong absorption between states near N_2 and N_1 (~ 1.3 eV) where the bands are very flat, as well as at 18 eV where final states of compatible symmetries exist both at N and H. The corresponding transitions calculated in the APW framework appear a few eV lower in energy. A complete calculation of the transition matrix elements is however required before more quantitative results can be presented. We note that the present estimate of the transition energies is not expected to accurately reflect the true optical elementary excitations, as the local density functional approach used here does not include self-interaction cancellation as well as self-energy (relaxation and correlation) effects.

The present calculation yields a density of states of 8.57 states/(Ry atom) at the Fermi energy. This should be compared with the similar values of 8.68 states/(Ry atom) obtained in the warped muffin-tin calculation of Koelling *et al.*[27] and 8.84 states/Ry atom obtained by Moruzzi *et al.*[29] Using the measured specific heat data of Roser *et al.*,[46] this suggests a Fermi-surface average λ value of 0.25. As pointed out by Koelling *et al.*,[27] this value is much smaller than that inferred from the McMillan equation (~ 0.40), using the observed transition temperature, Debye temperature, and isotope shift parameter.

C. Charge density

The bonding characteristics in Mo can be studied from the nature of the variational charge density. We first concentrate on the contribution of some high-symmetry points to the charge density (Figs. 5–7).

The bottom of the valence band in Mo (Γ_1) is a pure s state which is delocalized on a fairly large portion of the unit cell [Fig. 5(a)]. As one progresses towards the Fermi energy, d character is seen to be strongly admixed [Figs. 5(b), 6(a), and 6(c)]. There are two principal types of d bonding: the $\Gamma_{25'}$ state [Fig. 5(b)], the $H_{25'}$ [Fig. 6(a)], and the P_4 [Fig. 6(c)] are characteristic of the bonding type $d_{xy+yz+zx}$ in which four fairly localized d lobes are directed along the nearest-neighbor distance, whereas the H_{12} [Fig. 6(b)] and N_1 [Fig. 7(a)] states typify nonbonding d_{z^2} state (with some $d_{x^2-y^2}$ contribution, which is not seen in the plotting plane that forms a nodal x^2-y^2 plane) with its lobes pointing towards the *next*-nearest neighbors. The four equivalent maxima in the $d_{xy+yz+zx}$ states occur at a distance of about $\frac{1}{5}a$ from the atom (where a is the lattice constant) and constitute the largest non-muffin-tin contribution to the charge density within the "atomic sphere"

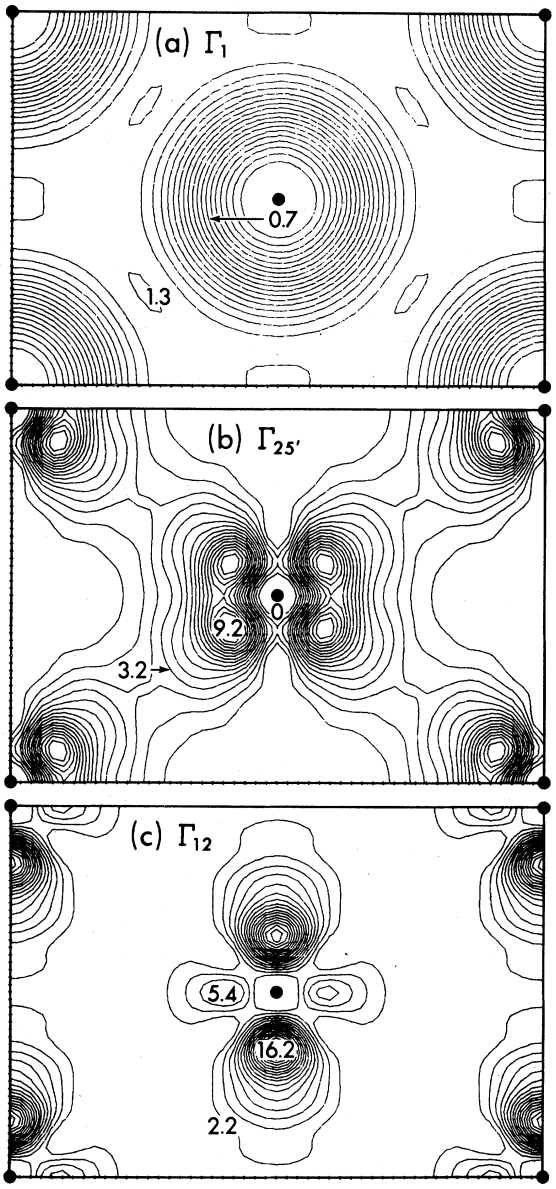

FIG. 5. Band charge density in Mo at the Γ point in the (110) plane. Full dots indicate atomic positions. Values are given in e/cell, normalized to unity; (a) Γ_1, (b) Γ_{25}, and (c) Γ_{12}.

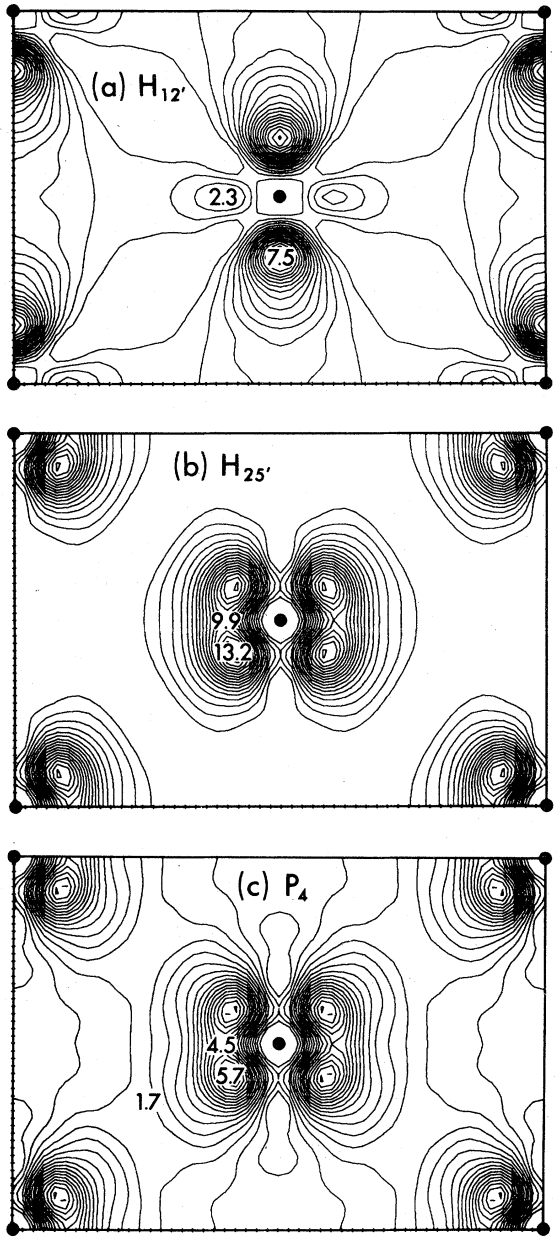

FIG. 6. Band charge density in Mo at the H and P points in the (110) plane. Full dots indicate atomic positions. Values are given in e/cell, normalized to unity; (a) H_{12}, (b) $H_{25'}$, and (c) P_4.

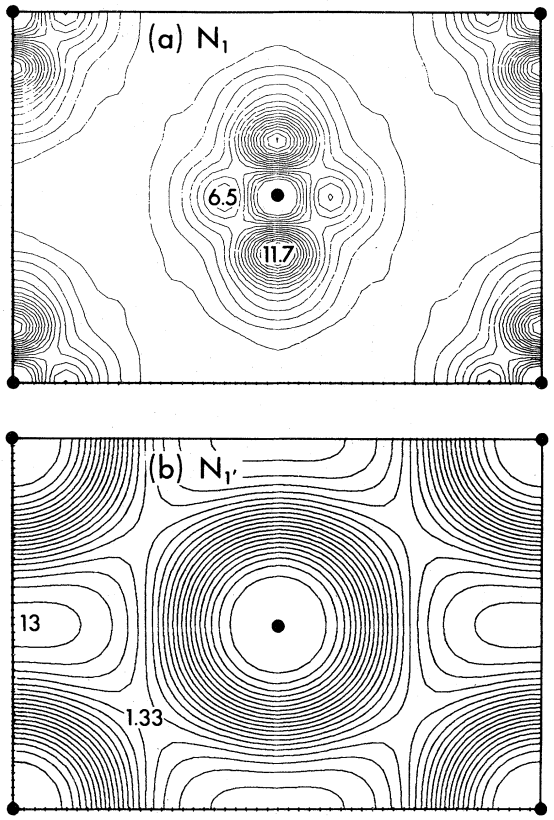

FIG. 7. Band charge density in Mo at the N point in the (110) plane. Full dots indicate atomic positions. Values are given in e/cell, normalized to unity; (a) N_1 (band 3), (b) $N_{1'}$ (band 4).

($\leq \frac{1}{2}a$).[24-27] The vicinity of the d-type states H_{12} and N_1 to the bottom of the s band induces some s-d hybridization into the former, characterized by shallow bond-oriented lobes [Figs. 6(b) and 7(a)]. A similar p-d hybridization occurs at the P_4 state [resulting in next-nearest neighbor directed lobes in Fig. 6(c)]. The basic bonding mechanism in this material stems therefore from localized bond-directed d orbitals interacting with an extended background of s and p states which hybridize with the d states at the band edges.

Above the Fermi energy, one encounters the nonbonding $d_{z^2}+d_{x^2-y^2}$ states of the Γ_{12} type [Fig. 5(c)] which strongly hybridize with states of p symmetry along the Γ-N direction. This is clearly seen at the $N_{1'}$ point [Fig. 7(b)] which constitutes a pure p state which delocalizes over most of the unit cell and similar states along the D and Σ directions (not shown).

The total valence pseudo charge density of Mo is shown in Fig. 8. Along with a metallic background at the cell boundaries, the localized features of the bond-oriented d states are clearly seen. The value of the charge maxima (4.3 e/cell) is significantly larger than the value previously obtained for W (3.0e),[36] in accord with the higher s-binding energy of Mo, associated with its deeper $l=0$ pseudopotential.[11]

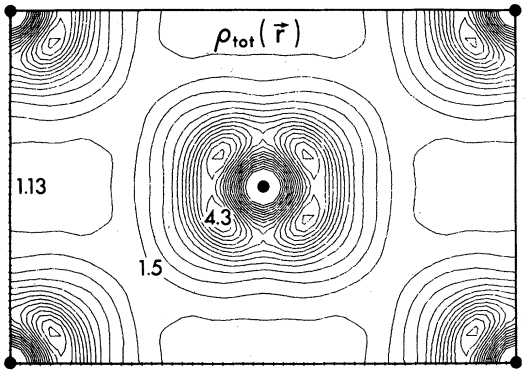

FIG. 8. Total valence pseudopotential charge density of Mo in the (110) plane.

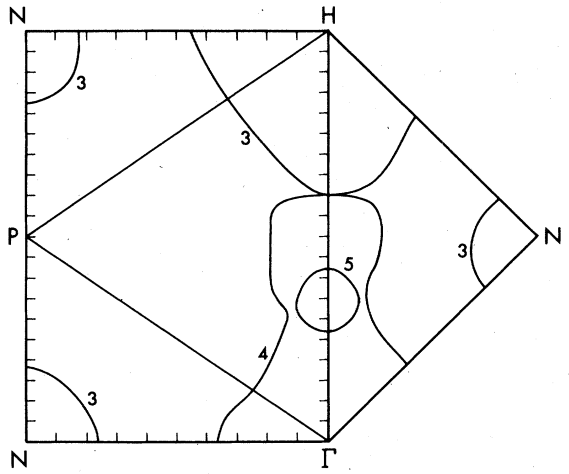

FIG. 9. Calculated cross sections of the Fermi surface in the (100) and (110) planes of Mo.

D. Fermi surface

Detailed theoretical and experimental studies of the Mo Fermi surface (FS) have been given by several authors. A relatively complete survey is presented in Ref. 27. We have used the results of our Fourier fit to obtain information about the Fermi-surface dimensions of Mo within the first-principles pseudopotential method in Fig. 9. We have plotted the cross section of the Fermi surface in the (100) and (110) planes in analogy to Ref. 27. Bands 3 – 5 contribute to the FS. Contribution of band 3 is purely hole-like and consists of an ellipsoid around N and an octahedron around H. Band 4 is an electronlike jack around Γ, finally band 5 contributes a small electronlike lens centered along the Δ-symmetry line which is nearly circular. In Table VI we compare the FS cross-section dimensions along high-symmetry directions with the calculations of Koelling *et al.*[27] obtained from a relativistic APW (RAPW) calculation, the results of Boiko *et al.*[47] obtained from the radio-frequency size effect (RFSE) and the results of Cleveland *et al.*[48] obtained from the de Haas–van Alphen (dHvA) effect. Considering the relatively small amount of primary points included in the Fourier fit the agreement is quite remarkable. We do not get, of course, a jack-octahedron separation because our calculation is nonrelativistic.

IV. CONCLUSIONS

The first-principles nonlocal pseudopotential method is shown to provide an accurate representation of the bulk electronic properties of molybdenum. Within this approach, the band structure, the density

TABLE VI. Fermi-surface cross-section dimension in Å^{-1} for Mo.

	Direction	This Work	Ref. 27 RAPW	Ref. 47 RFSE	Ref. 48 dHvA
Band 3 (hole)					
Octahedron	[100]	0.80	0.81	0.79	0.81
	[110]	0.66	0.60	0.60	0.61
N ellipsoid	$N\Gamma$	0.35	0.36	0.29	0.33
	NH	0.25	0.22	0.22	0.22
	NP	0.36	0.40	0.38	0.37
Band 4 (electron)					
Jack	[100]	1.20	1.15	1.16	1.10
	[110]	0.54	0.52	0.49	· · ·
Band 5 (electron	[100]	0.30	0.26	0.31	· · ·
Diameter		0.32	0.35	· · ·	· · ·

of states, charge density, and the Fermi surface can be reproduced in reasonable agreement with other calculations and experiment. Together with a mixed-basis representation of the crystal wave function which accounts for both the delocalized nature of the s and p electrons and the strong localization of the d electrons, this nonempirical self-consistent pseudopotential approach provides a very efficient technique for electronic-structure calculations.

ACKNOWLEDGMENTS

This work was supported in part by the Division of Basic Energy Science, U.S. DOE and NSF Grant DMR76-20647-A01. One of us (A.Z.) would like to thank the IBM Corporation for support.

---

*Present Address: Solar Energy Research Institute, Golden, Colorado, 80401.

†Present Address: Max Planck Institute für Festkorperforschung, 70000 Stuttgart 80, West Germany.

[1]M. L. Cohen and V. Heine, in *Solid State Physics,* edited by H. Ehrenreich, F. Seitz, and D. Turnbull (Academic, New York, 1970), Vol. 24, p. 38; D. Brust, in *Methods in Computational Physics,* edited by B. Alder, S. Fernbach, and M. Rotenberg (Academic, New York, 1968), Vol. 8, p. 33.

[2]C. Y. Fong and M. L. Cohen, Phys. Lett. A 44, 375 (1973).

[3]J. F. Alward, C. Guha Sridhar, C. M. Perlof, and C. Y. Fong, Phys. Rev. B 15, 5724 (1977).

[4]C. Y. Fong and M. L. Cohen, Phys. Rev. Lett. 24, 306 (1970).

[5]J. F. Alward, C. Y. Fong, and C. Guha Sridhar, Phys. Rev. B 18, 5438 (1978).

[6]K. M. Ho, S. G. Louie, J. R. Chelikowsky, and M. L. Cohen, Phys. Rev. B 15, 1755 (1977).

[7]G. P. Kerker, K. M. Ho, and M. L. Cohen, Phys. Rev. Lett. 40, 1593 (1978); and Phys. Rev. B 18, 5473 (1978).

[8]See W. A. Harrison, in *Pseudopotentials in the Theory of Metals* (Benjamin, New York, 1966).

[9]I. V. Abarenkov and V. Heine, Philos. Mag. 12, 529 (1965); V. Heine and I. V. Abarenkov, Philos. Mag. 9, 451 (1963).

[10]A. Zunger and M. Ratner, Chem. Phys. 30, 423 (1978).

[11]A. Zunger and M. L. Cohen, Phys. Rev. B 18, 5449 (1978).

[12]S. Topiol, A. Zunger, and M. Ratner, Chem. Phys. Lett. 49, 367 (1977).

[13]W. Kohn and L. J. Sham, Phys. Rev. 140, 1133 (1965).

[14]A. Zunger and M. L. Cohen, Phys. Rev. Lett. 41, 53 (1978); A. Zunger (unpublished).

[15]A. Zunger and M. L. Cohen, Phys. Rev. B (to be published); D. R. Hamann and A. Zunger (unpublished).

[16]About 50 plane waves are needed to converge the bulk Mo band structure to within 0.2 eV, using a mixed-basis representation and the semiempirical pseudopotential, Ref. 7 whereas a similar convergence for the first-principles pseudopotential requires about 70 plane waves. An accuracy of 0.05 eV requires 100 plane waves. Although the difference between the number of waves needed for the semiempirical potential and the first-principles one is rather immaterial for bulk (i.e., 1 atom per cell) transition-metal calculations, it becomes important for surface calculations with a repeated slab geometry, in which typically five atoms per cell have to be considered (Ref. 7). In this case, inclusion of more than a single Gaussian for the $l=2$ symmetry might be needed when the first-principles pseudopotential is used.

[17]G. P. Kerker, A. Zunger, M. L. Cohen, and M. Schlüter, Solid State Commun. (to be published).

[18]M. Schlüter, A. Zunger, G. P. Kerker, K. M. Ho, and M. L. Cohen, Phys. Rev. Lett. 42, 540 (1979).

[19]S. G. Louie, K. M. Ho, and M. L. Cohen (unpublished).

[20]R. N. Euwema, Phys. Rev. B 4, 4332 (1971).

[21]R. A. Deegan and W. D. Twose, Phys. Rev. 164, 993 (1967).

[22]A. B. Kunz, J. Phys. C 3, 1542 (1970).

[23]A. Zunger and M. L. Cohen, Phys. Rev. B 19, 568 (1979).

[24]T. M. Loucks, Phys. Rev. 139, 1181 (1965).

[25]I. Petroff and C. R. Viswanathan, Phys. Rev. B 4, 799 (1971).

[26]R. C. Cinti, E. Al Khoury, B. K. Chakraverty, and N. E. Christensen, Phys. Rev. B 14, 3296 (1976).

[27]D. D. Koelling, F. M. Muller, A. J. Arko, and J. B. Ketterson, Phys. Rev. B 10, 4889 (1974).

[28]R. J. Iverson and L. Hodges, Phys. Rev. B 8, 1429 (1973).

[29]V. Moruzzi, J. Janak, and A. R. Williams (private communication).

[30]W. E. Pickett and P. B. Allen, Phys. Rev. B 11, 3599 (1975).

[31]This point can be demonstrated using an atomic example. While both the model and the first-principles pseudopotentials are made to fit the all-electron properties well of the ground $4d^5 5s^1 5p^0$ configuration, when applied to *excited* configurations such as $4d^6 5s^0 5p^0$ or $4d^5 5s^0 5p^0$ (configuration which mimic to some extent typical perturbations on the atom when placed in a solid, such as $s \rightarrow p$ promotion and d orbital delocalization) notable differences occur: the first-principles pseudopotentials still fit the corresponding all-electron results to within 1% in the energy eigenvalues and 2% in the first moment of the wave function, whereas the model potential show discrepancies of 8% (i.e., 0.5 eV) and 12%, respectively. This can be traced to the large core penetration of the valence orbitals obtained with the model potential. Similar discrepancies exist in the bulk band structure as calculated with both potentials (e.g., when referred to the Fermi energy of the respective calculations, the differences are 0.1 eV for $\Gamma_{25'}$, 0.52 eV for $\Gamma_{12'}$, 0.34 eV for P_4, 0.47 eV for P_3, and 0.41 eV for N_2, the model potential results being consistently lower in energy).

[32]K. S. Singwi, A. Sjölander, P. M. Tosi, and R. H. Land, Phys. Rev. B 1, 1044 (1970).

[33]J. W. Cooley and J. W. Tukey, Math. Comput. 19, 297 (1965).

[34]The formalism is trivially adaptable to the choice of a more general V_L in terms of a linear combination of all U_l's. This can be used to obtain an arbitrarily smooth V_L in momentum space.

[35]D. J. Chadi and M. L. Cohen, Phys. Rev. B 8, 5747 (1973).
[36]A. Zunger and M. L. Cohen (unpublished).
[37]G. Lehman and M. Taut, Phys. Status Solidi 54, 469 (1971).
[38]P. O. Löwdin, Int. J. Quantum Chem. S 1, 811 (1967).
[39]L. Hodges, R. E. Watson, and H. Ehrenreich, Phys. Rev. B 5, 3953 (1972).
[40]K. A. Kress and G. J. Lapeyre, Nat. Bur. Stand. (U.S.), Spec. Publ. 323, 209 (1971).
[41]D. E. Eastman, Solid State Commun. 7, 1697 (1969).
[42]M. M. Kirilova, L. M. Nomerovannaya, and M. M. Noskov, Zh. Eksp. Teor. Fiz. 60, 2252 (1971) [Sov. Phys. JETP 33, 1210 (1971)].
[43]M. L. Kapitsa, Yu. P. Udoyev, and E. I. Shirokikh, Fiz. Tverd. Tela (Leningrad) 11, 816 (1969) [Sov. Phys. Solid State 665 (1969)].
[44]B. W. Veal and A. P. Paulikas, Phys. Rev. B (to be published).
[45]J. H. Weaver, D. W. Lynch, and C. G. Olson, Phys. Rev. B 10, 501 (1974).
[46]D. C. Roser, D. G. Onn and H. Meyer, Phys. Rev. 138, A1661 (1965).
[47]V. V. Boiko, V. A. Gaspanov, and I. G. Gverdtsiteli, Zh. Eksp. Teor. Fiz. 56, 489 (1969) [Sov. Phys. JETP 29, 267 (1969)]; V. V. Boiko and V. A. Gasparov, *ibid,* 61, 1976 (1971) [*ibid,* 34, 1054 (1972)].
[48]J. R. Cleveland and J. L. Stanford, Phys. Rev. B 4, 311 (1971).